JOURNAL OF SOLID STATE CHEMISTRY 94, 337–351 (1991)

A Conventional and High-Resolution Synchrotron X-Ray Diffraction Study of Phase Separations in $Pr_2NiO_{4+\delta}$

J. D. SULLIVAN AND D. J. BUTTREY

Department of Chemical Engineering, University of Delaware, Newark, Delaware 19716

AND D. E. COX AND J. HRILJAC

Physics Department, Brookhaven National Laboratory, Upton, New York 11973

Received March 8, 1991; in revised form June 3, 1991

Several $Pr_2NiO_{4+\delta}$ samples with varying oxygen content have been examined by conventional and high-resolution synchrotron X-ray powder diffraction techniques. Three different phase separation regions have been identified with synchrotron diffraction, and the room temperature lattice parameters of each phase are reported, as well as conventional X-ray powder diffraction data on four single-phase regions of the phase diagram. The low temperature behavior of a sample with an average excess oxygen content of 0.020 was also studied, revealing phase coexistence and a tetragonal to orthorhombic phase transition on heating at 118 K. A semiquantitative oxygen concentration phase diagram is proposed on the basis of the amount of excess oxygen in the individual phases, as estimated from iodometric titrations and relative phase volumes. In addition, the overall stability field of $Pr_2NiO_{4+\delta}$, showing the oxygen fugacity at the reduction and oxidation boundaries as a function of temperature, is reported.

Introduction

The influence of oxygen nonstoichiometry on the structure and physical properties of $Ln_2MO_{4+\delta}$ layered oxides (Ln = La, Pr, Nd; M = Cu, Ni, Co) has been studied extensively since the discovery of high-T_c superconductivity. Deviations from ideal oxygen stoichiometry among these oxides of the K_2NiF_4 structure-type are directly associated with significant changes in structural distortions and physical behavior, often manifested by the phase separation of defects, and for some compositions, the appearance of high-T_c superconductivity. The separation of oxygen defects into two distinct phases, due to correlations of the interstitial ions and/or the holes generated for charge compensation, has been reported in $La_2MO_{4+\delta}$ (*1–3*) and $Pr_2NiO_{4+\delta}$ (*4*). Even though these phase separations have been reported to occur over different ranges of oxygen stoichiometry for different oxides, it is expected that the location and correlation of the oxygen defects are similar among isostructural oxides. The interstitial nature of the excess oxygen was identified by density measurements on $Pr_2NiO_{4+\delta}$ and $La_2NiO_{4+\delta}$ (*5*), and by neutron diffraction with $La_2CuO_{4+\delta}$ (*6*) and $La_2NiO_{4+\delta}$ (*2*). Neutron

0022-4596/91 $3.00

single-crystal diffraction experiments by Chaillout *et al.* (*6*) on the oxygen-rich superconducting phase of $La_2CuO_{4+\delta}$ reveal that the oxygen defect is in the (1/4, y = 0.243, 1/4) interstitial site at 15K. Neutron powder data obtained by Jorgensen *et al.* (*2*) on the oxygen-rich phase of $La_2NiO_{4+\delta}$ also show the oxygen defect site to be near the (1/4, 1/4, 1/4) interstitial position of the $\sqrt{2}a \times \sqrt{2}b \times c$ K_2NiF_4 supercell. In order to minimize the charge separation between layers in these materials, it is expected that the additional oxygen is interstitially incorporated as either an oxide ion or a peroxide species (cf. *5,2*). The locations of the defect sites in the lower oxygen excess phases of these materials have yet to be established, primarily because of very weak coherent scattering from the low defect concentrations in these species. In addition to their association with the phase separations observed in many of these oxides, the interstitial oxygen defects also cause dramatic changes in physical properties. $La_2CuO_{4+\delta}$ becomes superconducting with high concentrations of excess oxygen (cf. *1*), and the magnetic ordering of both copper and nickel oxides is strongly dependent upon oxygen stoichiometry (cf. *7*). For example, the Néel temperature of $Pr_2NiO_{4+\delta}$ decreases from well above 300 K at the stoichiometric limit to less than 5 K at high excess oxygen concentrations (*4, 8–10*). Although there are numerous examples of the effect of oxygen nonstoichiometry on layered oxides, it is difficult to quantify its relationship to physical properties because of the presence of coexisting phases. With the oxygen stoichiometry phase diagram more fully characterized, it is possible to systematically isolate, synthesize, and characterize the properties of each phase.

In this investigation we attempt to elucidate more clearly the role of excess oxygen in $Pr_2NiO_{4+\delta}$ phase equilibria by examining several different oxygen defect compositions by high-resolution synchrotron X-ray powder diffraction techniques. As with other layered oxides, the properties of $Pr_2NiO_{4+\delta}$ are highly dependent on synthesis conditions, with the amount of excess oxygen in the lattice established by the equilibrium annealing temperature and oxygen fugacity (the fugacity is equivalent in magnitude to the oxygen partial pressure under conditions used here). A more complete review of the previous work on $Pr_2NiO_{4+\delta}$ is given in a paper on a neutron single-crystal diffraction study (*4*) of phase separation and magnetic behavior in $Pr_2NiO_{4.020}$ and $Pr_2NiO_{4.060}$. In the neutron study, phase coexistence in $Pr_2NiO_{4.020}$ at room temperature is reported, as well as a transition at 118 K from tetragonal $P4_2/ncm$ symmetry to orthorhombic *Pccn* symmetry on heating. The same structural transition is observed here with high-resolution synchrotron X-ray diffraction, but now revealing two tetragonal phases with nearly identical unit cell parameters coexisting below the transition temperature. The reported miscibility gap was confirmed in this study by a second sample with slightly more excess oxygen showing the same coexistent phases in different proportions. We also report two additional miscibility gaps in the phase diagram which were identified in samples with even larger oxygen excess. One of the new phase separation regions contains the previously observed tetragonal phase coexisting with a more nonstoichiometric orthorhombic phase, whereas the most nonstoichiometric region contains two distinct orthorhombic phases. The characterization of nearly stoichiometric $Pr_2NiO_{4+\delta}$ is under continuing investigation due to the observation of complex structure–temperature dependences and multiple phases in some samples. The initial focus of this investigation was to construct a preliminary oxygen stoichiometry phase diagram by identifying the various areas of phase separation for $Pr_2NiO_{4+\delta}$, and to subsequently synthesize single-phase samples. The correlation

of this diagram with the structure and physical properties of the samples will allow a better understanding of the behavior of excess oxygen in $Pr_2NiO_{4+\delta}$ and other layered oxides. $Pr_2NiO_{4+\delta}$ appears to be a model system for studying the evolution of the complex oxygen concentration phase diagrams of layered perovskite oxides because of the large oxygen solubility range and the multiple regions of phase separation.

Experimental

$Pr_2NiO_{4+\delta}$ samples were prepared initially by solid–solid reaction in nickel crucibles of 99.995% NiO and 99.99% Pr_6O_{11} at 1470 K in air. The resulting sintered product was then used for either ceramic powder anneals, or as the starting material for crystal growth by radio frequency induction skull melting under a controlled oxygen atmosphere. Although this method of crystal growth can produce crystals of $Pr_2NiO_{4+\delta}$ as large as 0.7 cm^3 in volume, the typical crystals used in this investigation were approximately 0.005 to 0.012 cm^3, with a Pr/Ni ratio of 2.00 ± 0.01 as determined by EDTA titrations. Further details of the crystal growth procedure and general characterization of the single crystals are described elsewhere (*11, 12*).

The magnitude of oxygen nonstoichiometry of the single crystals of $Pr_2NiO_{4+\delta}$ was fixed through extended anneals under conditions of controlled oxygen fugacity and temperature. The oxygen fugacity of these subsolidus anneals was monitored by an Y_2O_3–ZrO_2 solid electrolyte cell calibrated against the Ni/NiO reduction boundary. The desired oxygen fugacities were achieved by flowing research purity gases (controlled by a Vacuum General Dynamass mass flow controller) through a closed system 1300°C Applied Test Systems tube furnace. CO/CO_2 buffers were used to maintain partial pressures of oxygen between 10^{-5} and 10^{-8} atm, whereas mixtures of Ar and O_2 were used for more moderate oxygen pressures (10^{-3} to 1 atm). All samples were annealed at 1470 K for 7 to 10 hr to ensure sufficient time for the equilibration of oxygen between the sample and the annealing environment. Samples were rapidly quenched to room temperature within the annealing atmosphere, and immediately stored in mineral oil to avoid any significant exchange of oxygen with the surroundings, which has been shown to occur with nearly stoichiometric samples of $La_2NiO_{4+\delta}$ even at room temperature (*2*). Samples quenched and stored in this manner usually give diffraction peaks which are resolution-limited, even with high-resolution synchrotron X-ray diffraction techniques, except in some instances where strain or intrinsic disorder appear to be present. Oxygen-18 exchange experiments in $La_2NiO_{4+\delta}$ are currently in progress (*13*) to probe the complex relationships between oxygen diffusivity, temperature, and nonstoichiometry. Preliminary results of this study for a sample with $\delta \approx 0.05$ show significant exchange of interstitial oxygen sites beginning above 750 K, and a rapid exchange between all oxygen sites above 1050 K.

The excess oxygen concentration of samples from each anneal was determined by multiple iodometric titrations with deaerated sodium thiosulfate solutions in a nitrogen-filled glove box. The concentrations of the thiosulfate solutions were optimized with respect to the anticipated oxygen nonstoichiometry and sample size, with each solution calibrated against primary standard arsenic sesquioxide solutions prior to use. Blanks were also titrated with each sample, showing a negligible or small background requiring no more than a 2% correction in titrated volumes, apparently due to trace amounts of residual oxygen in the solutions. Three to four titrations were performed on 100- to 200-mg samples from each anneal. For this synchrotron X-ray study, $Pr_2NiO_{4+\delta}$ crystals were examined from controlled an-

TABLE I
EXCESS OXYGEN CONTENT OF ANNEALS OF $Pr_2NiO_{4+\delta}$

Temp (K)	log f_{O_2}	$\bar{\delta}$
1305	−0.00	0.215 ± 0.008[a]
1470	−0.00	0.195 ± 0.006
1305	−1.40	0.17 ± 0.01[a]
1470	−2.02	0.162 ± 0.007
1465	−3.25	0.064 ± 0.009[a]
1470	−4.99	0.052 ± 0.003
1470	−7.53	0.020 ± 0.001
1373	−9.35	<0.003[a,b]
1470	−8.00	<0.003[b]
1470	−8.18	<0.003[b]

[a] Single-phase specimen.
[b] No titratable color was observed in these analyses; therefore, based on the sample masses, we estimate only an upper bound on $\bar{\delta}$. In the absence of color change we are unable to draw any conclusions as to whether or not any of these specimens is substoichiometric.

neals at 1470 K, under equilibrium oxygen fugacities of log f_{O_2} = 0.00, −2.02, −4.99, −7.53, −8.00, and −8.18. The samples were chosen to be within the phase separation regions, requiring the iodometric titration results to be reported in terms of an average oxygen nonstoichiometry, $\bar{\delta}$, which will subsequently be used to identify each of the samples. The synchrotron results allowed the preparation of four single-phase samples, which were examined with conventional X-ray powder diffraction techniques and also titrated. The results of the iodometric titrations of all samples are summarized in Table I.

Synchrotron X-ray powder diffraction measurements were carried out at the Brookhaven National Synchrotron Light Source (NSLS), on beamline X7A. Annealed crystals of $Pr_2NiO_{4+\delta}$ were ground in a nitrogen-filled glove box to produce the powder samples. The ground samples were mounted on a flat plate sample holder and were then mounted in a closed cycle helium (Displex) refrigerator with berylium windows. Data were collected on the sample $\bar{\delta}$ = 0.020 using a channel cut Si(111) monochromator and a linear position-sensitive detector at a wavelength of 0.7662(3) Å. Subsequent data were collected using the Si monochromator with a Ge(220) analyzer crystal at a wavelength of 1.19992(2) Å. Wavelengths were established by calibration against a reference sample of CeO_2. Some samples showed preferred orientation and/or texturing effects because of the difficulty of grinding single crystals into a small, uniform particle size powder. Larger crystalline particles may contribute anomalously to the normal Voigt peak shape, causing a jagged reflection, which may add to uncertainties in lattice parameter refinements. However, the more homogeneous and pure $Pr_2NiO_{4+\delta}$ samples available with single crystals compared to samples prepared by conventional ceramic techniques far outweigh the disadvantages caused by texture effects. Conventional X-ray powder diffraction experiments were carried out with an automated Philips APD 3520 diffractometer with Cu$K\alpha$ radiation.

Results

Overall Stability Field for $Pr_2NiO_{4+\delta}$

While preparing samples for this X-ray synchrotron study, we also characterized the $f_{O_2} - T$ dependence for the overall stability field of $Pr_2NiO_{4+\delta}$ with conventional X-ray diffraction techniques. It is necessary to use crystals instead of powder samples for the determination of the stability boundaries, because diffusivity of oxygen in a finely divided powder is not insignificant relative to the time scale for quenching. This becomes a problem near the limits of the stability field, where very small changes in oxygen stoichiometry can lead to reduction or oxidation of the sample during the quench

(when the sample is removed from the equilibrium environment and cooled to room temperature). Crystals are used to avoid this problem, as their large volume to surface area ratio results in a characteristic diffusion time that is much greater than the quench time. The reduction boundary of the stability field (i.e., the conditions for preparing stoichiometric material) was initially found by annealing crystals at 1470 K under increasingly reducing atmospheres until the formation of reduction products was observed. Samples annealed at or below log $f_{O_2} = -8.20$ at 1470 K reduced to form nickel metal and Pr_2O_3. The sample annealed at log $f_{O_2} = -8.18$ also contained minor amounts of Ni° and Pr_2O_3, indicating the immediate proximity of the reduction boundary. Samples annealed at log $f_{O_2} = -8.15$ showed no traces of reduction products. Subsequent anneals at 1373 and 1223 K allowed determination of the f_{O_2}-temperature dependence of the lower boundary, which is approximated by the van't Hoff equation

$$\log f_{O_2}(\text{atm}) = -24{,}158/T + 8.206. \quad (1)$$

The oxidation boundary of the overall stability field was found by annealing crystals under increasingly oxidizing atmospheres until the formation of oxidation products were observed. Crystals annealed in pure oxygen below 1303 K oxidized to form $PrO_{1.83}$ and the multilayered perovskite $Pr_4Ni_3O_{10}$, with no evidence of other layered phases such as $Pr_3Ni_2O_7$. The oxidation boundary reaction is

$$3Pr_2NiO_{4+\delta} + aO_2 \Leftrightarrow Pr_4Ni_3O_{10+\delta'} + 2PrO_{1.83+\delta''}, \quad (2)$$

where $a = 0.83 + 0.50\delta' + \delta'' - 1.50\delta$. If we assume that δ' and δ'' are negligible, and that the maximum oxygen excess of $Pr_2NiO_{4+\delta}$ is approximately 0.22, then $a = 0.50$. Using the results of anneals at 1303, 1229, and 1178 K, the temperature dependence of the oxidation boundary may be approximated by the van't Hoff equation

$$\log f_{O_2}(\text{atm}) = -3679/T + 2.828. \quad (3)$$

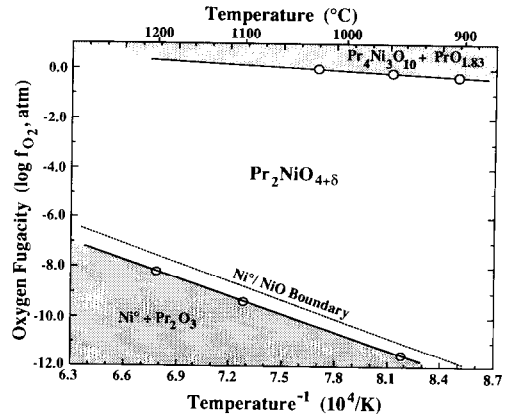

FIG. 1. Stability field for $Pr_2NiO_{4+\delta}$, showing the f_{O_2}-temperature dependence of the reduction and oxidation boundaries, as well as the reduction boundary of NiO/Ni° for reference.

Both boundaries of the stability field are plotted in Fig. 1, along with a dashed line showing the Ni°/NiO boundary for reference. The full-width-half-maximum of Bragg reflections of $Pr_4Ni_3O_{10}$ (as formed from the oxidation $Pr_2NiO_{4+\delta}$) are extremely broad, indicative of a very small particle size. The approximate lattice parameters for $Pr_4Ni_3O_{10}$, as determined from conventional X-ray powder diffraction on a ceramic $Pr_2NiO_{4+\delta}$ sample annealed in 1 atm of oxygen at 1223 K, are $a = 5.373(9)$, $b = 5.465(9)$, and $c = 27.53(3)$. A ceramic sample was used in an attempt increase the reaction kinetics and to produce $Pr_4Ni_3O_{10}$ with a uniform particle size. A selected region of this diffraction pattern has been indexed and is presented in Fig. 2, showing reflections from both $Pr_4Ni_3O_{10}$ and $PrO_{1.83}$ (a trace amount of NiO is also present due to incomplete reaction in the ceramic $Pr_2NiO_{4+\delta}$ syn-

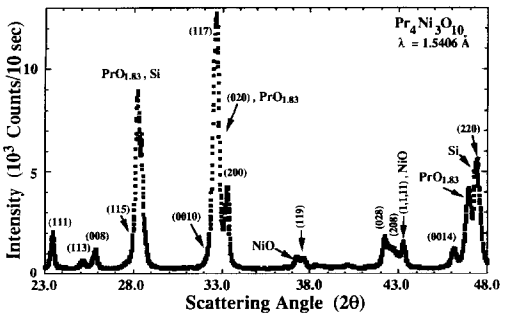

FIG. 2. Selected portion of the diffraction pattern of the oxidation products from a ceramically prepared $Pr_2NiO_{4+\delta}$ specimen annealed at 1223 K in oxygen. Both the multilayered perovskite $Pr_4Ni_3O_{10}$ and $PrO_{1.83}$ are observed, as well as an internal silicon standard and residual NiO from the ceramic preparation.

thesis). $PrO_{1.83}$ has previously been characterized by Swanson *et al.* (*14*).

Structural Symmetries of $Pr_2NiO_{4+\delta}$ Phases

Conventional and synchrotron X-ray diffraction data on $Pr_2NiO_{4+\delta}$ were indexed on the basis of the $\sqrt{2}a \times \sqrt{2}b \times c$ supercell of the idealized body-centered tetragonal K_2NiF_4-type parent structure, preserving c as the long axis and a as the shortest axis. On the basis of previous work on $Pr_2NiO_{4+\delta}$, the structures of samples in this study are expected to have symmetries that are Landau subgroups of the parent space group, $I4/mmm$. The expected subgroup symmetries include *Bmab*, $P4_2/ncm$, *Pccn*, and *Fmmm*. The distortions associated with these symmetries involve the systematic canting of NiO_6 octahedra about fixed rotation axes which are parallel to the basal plane. *Bmab*, $P4_2/ncm$, and *Pccn* symmetries are distinguished from each other by nearest neighbor corner-shared octahedra canting in opposite directions about rotation axes parallel to ⟨100⟩, ⟨110⟩, or a linear combination of the two, respectively. The azimuthal orientation of the rotation axes for neighboring planes of octahedra differ by 90° in the $P4_2/ncm$ symmetry, 0° in *Bmab*, and between 0 and 90° in *Pccn*. These symmetries are also characterized by long range order of the octahedral canting. When disorder is present, or the correlation length of the canting is short, the resulting average structure is best described by *Fmmm* symmetry. The *Fmmm* symmetry may also be the result of assigning an average structure to a material with uncharacterized incommensurate order or the presence of a weak supercell with dimensions exceeding the $\sqrt{2}a \times \sqrt{2}b \times c$ cell.

All $Pr_2NiO_{4+\delta}$ samples examined in the synchrotron X-ray study contained coexisting phases, with the two that were annealed in very close proximity to the reduction boundary containing a nonequilibrium assemblage of K_2NiF_4-type phases, as well as trace amounts of Ni° and Pr_2O_3. Along with the phase separation previously reported for $Pr_2NiO_{4+\delta}$ (*4*), two additional phase separation regions with larger nonstoichiometries were also identified. The three phase separation regions consist of pairs from among four distinct phases, all of which have been subsequently synthesized and characterized with conventional X-ray diffraction techniques. The conventional X-ray data on the phase pure specimens are presented first, to justify the symmetry assignments in the synchrotron X-ray study. The two most nonstoichiometric $Pr_2NiO_{4+\delta}$ phases have both been assigned *Fmmm* symmetry, with the most nonstoichiometric phase being labeled *Fmmm*(2) and the other *Fmmm*(1). Although one or both of these phases may be isostructural with the nonstoichiometric $La_2CuO_{4+\delta}$ phase of *Cmca* symmetry (*6*, *15*), most of the superlattice reflections, which are generally observed only in neutron diffraction patterns, were unobserved, necessitating the assignment of the higher symmetry space group. Selected portions of the conventional X-ray diffraction patterns of the *Fmmm* phases are presented in Figs. 3 and 4, showing the orthorhombic splitting

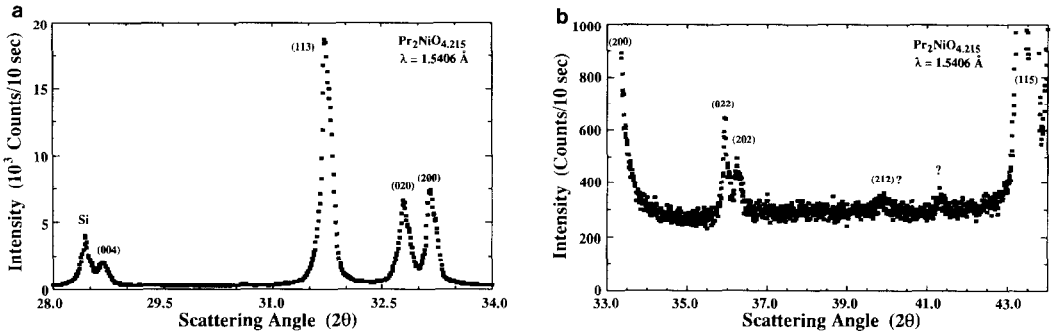

FIG. 3. Selected portions of the diffraction pattern of single-phase $Pr_2NiO_{4.215}$ (*Fmmm*(2)) annealed at 1305 K in oxygen. The lattice parameters for this sample are a = 5.400(3), b = 5.455(3), and c = 12.442(5). The strong reflections in (a) show the orthorhombic splitting, and the weak superlattice reflections observed in (b) suggest a symmetry lower than *Fmmm*, although no obvious indices could be identified.

of the (200)-type reflections, as well as a region where superlattice reflections may be expected. Despite the appearance of two small superlattice reflections for the most nonstoichiometric phase, and the anomalously high background in the *Fmmm*(1) pattern, we still assign *Fmmm* symmetry because of the very weak intensity and unassigned indices of some superlattice reflections, and the absence of additional expected superlattice reflections. High-resolution neutron and further synchrotron X-ray diffraction studies are planned to determine if the structures may be described by a larger unit cell or a lower symmetry space group. The X-ray diffraction pattern of a $\delta \approx 0.064(9)$ single-phase specimen with $P4_2/ncm$ symmetry, similar to that previously reported (*4*), is presented in Fig. 5, clearly showing the expected superlattice reflections. Figure 6 shows the diffraction pattern of stoichiometric $Pr_2NiO_{4.000(3)}$, which is consistent with an orthorhombic phase of either *Pccn* or *Bmab* symmetry. Although

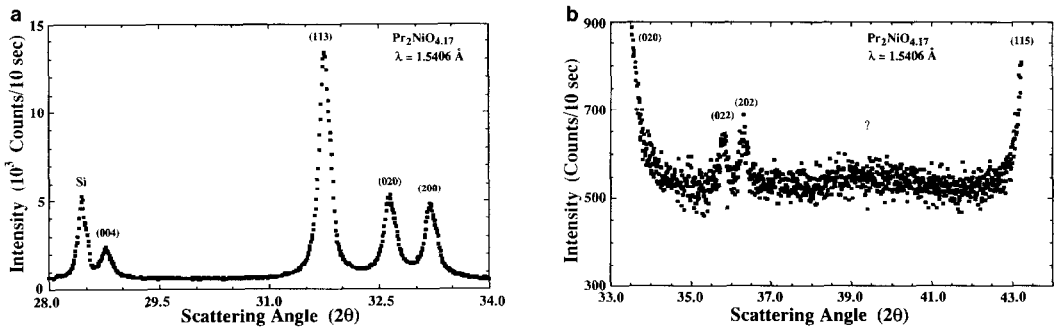

FIG. 4. Selected portions of the diffraction pattern of single-phase $Pr_2NiO_{4.17}$ (*Fmmm*(1)) annealed at 1305 K at $\log f_{O_2} = -1.40$. The lattice parameters for this sample are a = 5.393(4), b = 5.483(4), and c = 12.411(6). The orthorhombic splitting (a) is larger than that observed for *Fmmm*(2), and the anomalously high background around 39° suggests that very weak superlattice reflections may be present.

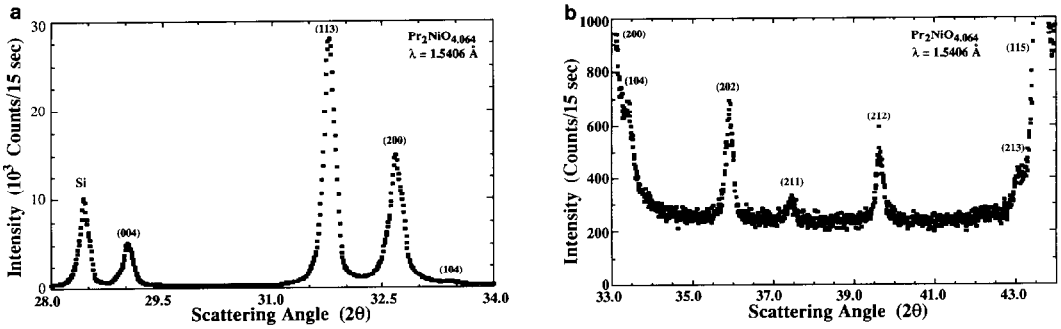

FIG. 5. Selected portions of the diffraction pattern of single-phase $Pr_2NiO_{4.064}$ annealed at 1473 K at log f_{O_2} = −3.25. The lattice parameters for this sample are a = 5.475(1) and c = 12.292(4). No orthorhombicity is evident in (a), and the observed superlattice reflections in (b) are consistent with $P4_2/ncm$ symmetry.

Pccn symmetry is expected from previous neutron diffraction experiments, it cannot be unambiguously distinguished from *Bmab* symmetry with conventional or synchrotron radiation under our experimental conditions because of the near-zero intensity of key superlattice reflections. These single-phase $Pr_2NiO_{4+\delta}$ samples are the basis of an oxygen concentration phase diagram which will be presented and discussed later in the paper.

Synchrotron X-Ray Diffraction

The $Pr_2NiO_{4+\delta}$ samples examined with synchrotron X-ray diffraction are labeled with respect to their average oxygen nonstoichiometry, with the results presented beginning with the most nonstoichiometric and ending with the most stoichiometric sample. The most nonstoichiometric sample, $\bar{\delta}$ = 0.195, contains two coexisting orthorhombic phases which have both been assigned *Fmmm* symmetry. Again, since some very weak superlattice reflections were observed but not unambiguously assigned, these phases may be expected to be of lower symmetry. Data were obtained only at 300 K, from which lattice parameters of a = 5.4008(4), b = 5.4587(5), and c = 12.4387(7) for the more nonstoichiometric *Fmmm*(2) phase and a = 5.3891(4), b = 5.4830(5), and c = 12.4202(7) for the *Fmmm*(1) phase were determined. The assignment of higher and lower nonstoichiometric phases is possible because the *Fmmm*(1) phase is also present in a lower $\bar{\delta}$ sample, whereas the most nonstoichiometric phase (*Fmmm*(2)) is not. Based on the relative intensities of the (200)-type reflections (Fig. 7a), the *Fmmm*(1) phase is estimated to comprise 60% of the $\bar{\delta}$ = 0.195 sample. The error in the relative phase volume may be as large as 10% due to the differences in scattered intensity among the various phases and from texturing effects. Although most of the diffraction peaks from this sample are resolution limited, the (0k0) reflections of both *Fmmm* phases are slightly broadened, which may be indicative of domains or intrinsic disorder in the (010) planes.

A second phase separation region is observed in the specimen with $\bar{\delta}$ = 0.162, consisting of the *Fmmm*(1) phase and a tetragonal $P4_2/ncm$ phase of lower nonstoichiometry. The room temperature lattice parameters for the coexisting phases of $\bar{\delta}$ = 0.162 are found to be a = 5.3940(4), b = 5.4853(4), and c = 12.4115(7) for the *Fmmm* phase, and a = 5.4706(6) and c = 12.3149(8) for the tetragonal phase. The assignment of

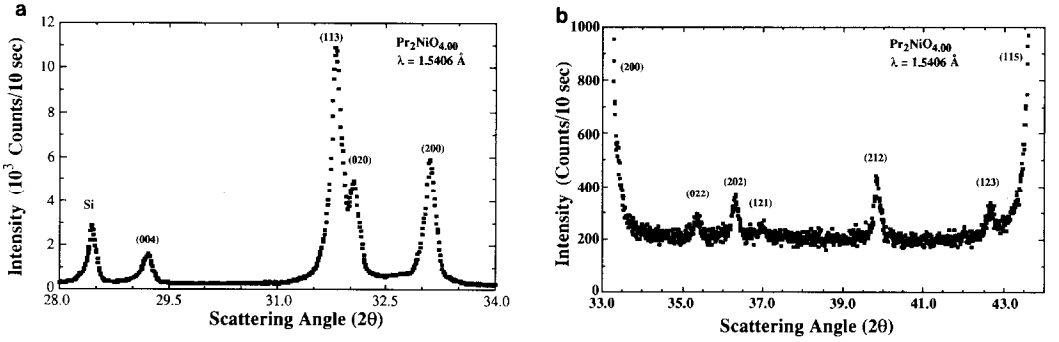

FIG. 6. Selected portions of the diffraction pattern of single phase $Pr_2NiO_{4.00}$ annealed at 1373 K at log $f_{O_2} = -9.35$. The lattice parameters for this sample are $a = 5.407(3)$, $b = 5.580(3)$, and $c = 12.221(7)$. The large orthorhombicity of the *Pccn* phase is shown in (a), with the corresponding superlattice reflections presented in (b).

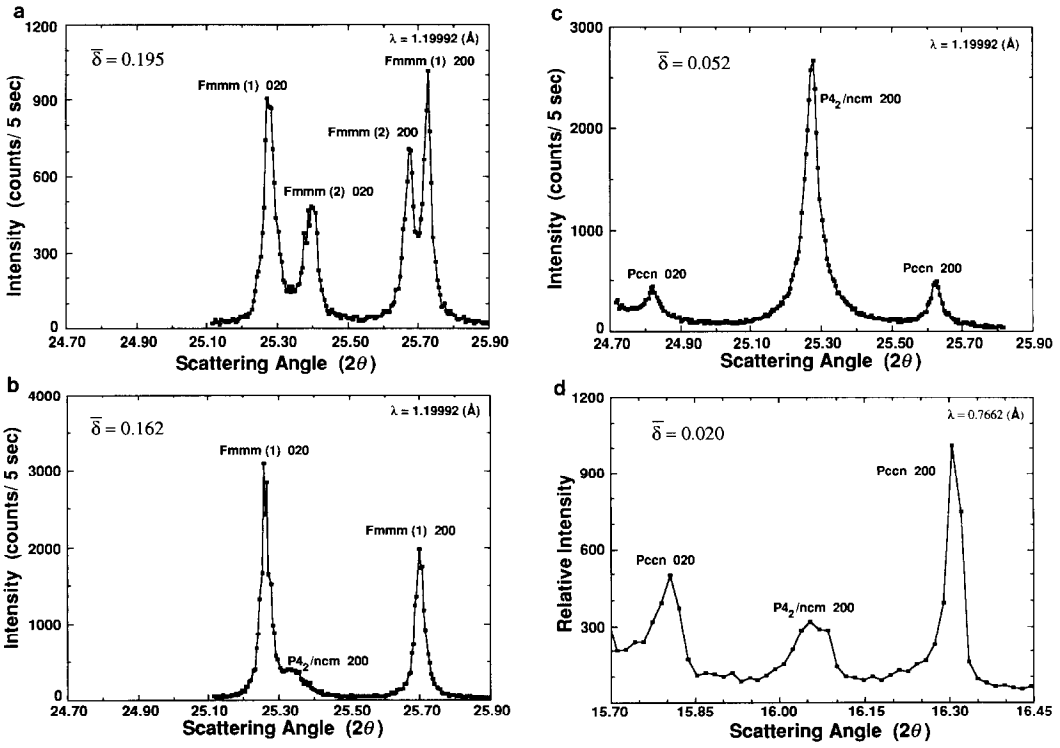

FIG. 7. (200)-type reflections showing phase coexistence for $Pr_2NiO_{4+\delta}$ samples with (a) $\bar{\delta} = 0.195$, (b) $\bar{\delta} = 0.162$, (c) $\bar{\delta} = 0.052$, and (d) $\bar{\delta} = 0.020$. Figures are scaled with respect to wavelength to yield the same range of d spacings despite different ranges of 2θ.

Fmmm(1) as the more nonstoichiometric phase is consistent with our previous study of a phase-pure $P4_2/ncm$ sample with an excess oxygen content of 0.060 (*4*). The relative intensities of the (200)-type reflections (as seen in Fig. 7b) indicate that the orthorhombic phase comprises approximately 85% of this sample.

A third phase separation region consisting of a tetragonal and an orthorhombic phase, which two of us previously reported in a neutron diffraction study (*4*) of $Pr_2NiO_{4.020}$, was also observed with synchrotron radiation for both $\bar{\delta} = 0.052$ and $\bar{\delta} = 0.020$. The phases in these samples are consistent with a tetragonal $P4_2/ncm$ phase and an orthorhombic phase of either *Pccn* or *Bmab* symmetry. The observed lattice parameters at 300 K for $\bar{\delta} = 0.052$ are $a = 5.4840(5)$ and $c = 12.2680(8)$ for the tetragonal phase and $a = 5.4089(6)$, $b = 5.5821(8)$, and $c = 12.228(2)$ for the orthorhombic phase. The observed lattice parameters at 300 K for $\bar{\delta} = 0.020$ are $a = 5.4811(7)$ and $c = 12.268(2)$ for the tetragonal phase and $a = 5.4077(4)$, $b = 5.5789(5)$, and $c = 12.2240(8)$ for the orthorhombic phase. The close agreement of the lattice parameters between samples is consistent with both samples being inside a single miscibility gap, and these X-ray parameters are also consistent with those reported for this phase separation region in the neutron study. Small deviations in the lattice parameters among the samples may be due to strain resulting from the lattice mismatch between phases, and to limitations in refining a two-phase assemblage, particularly when texturing effects are present. In contrast to the neutron study, the higher resolution synchrotron data have allowed us to deconvolute and assign the (00*l*) reflections. Again, the assignment of the tetragonal $P4_2/ncm$ phase as the more nonstoichiometric phase is in accord with earlier work and further verified by the proportions of the two phases in each sample. The relative intensities of the (200)-type reflections in the $\bar{\delta} = 0.052$ sample indicate that the tetragonal phase accounts for almost 90% of the sample (Fig. 7c), whereas the reflections $\bar{\delta} = 0.020$ suggest that this sample is only about 30% tetragonal (Fig. 7d).

In order to corroborate and more clearly interpret the neutron diffraction data on $Pr_2NiO_{4.020}$, synchrotron X-ray data were also obtained below room temperature on this sample. The temperature dependences of the lattice parameters for each phase are plotted in Fig. 8a, revealing two distinct phases below the first-order structural transition at 118 K, and distinct *c* parameters for all temperatures (Fig. 8b). These parameters are in general agreement with the neutron data, provided a weighted average of the *c* parameters is compared to the neutron results. Below the structural transition, two separate tetragonal $P4_2/ncm$ phases can be resolved, with the observed lattice parameters of these phases at 19 K being $a = 5.4863(5)$ and $c = 12.1946(9)$ for the original tetragonal phase, and $a = 5.4996(5)$ and $c = 12.1457(8)$ for the transformed tetragonal phase. Figure 9 shows the distinct (400) reflections for each tetragonal phase at 19 K. Fernandez-Diaz *et al.* (*16*) have reported a similar transition for stoichiometric $Pr_2NiO_{4+\delta}$ ($\delta \approx 0$) from an orthorhombic to a tetragonal phase at 115 K, except that they refine the low temperature phase to have correlated local *Pccn* symmetry because of a systematic broadening of certain reflections. In our data, most reflections appear to be near the instrument resolution limit, which necessitates refinement in $P4_2/ncm$ symmetry. The temperature dependences of the lattice parameters and the unit cell volumes of both phases are small and relatively linear, except on heating through the 118 K transition, where all parameters show a marked change. The orthorhombic strain shows a maximum at the 118 K transition, and sharply decreases just above the structural transition (Fig. 10), primarily due to a significant decrease in the *b* parameter

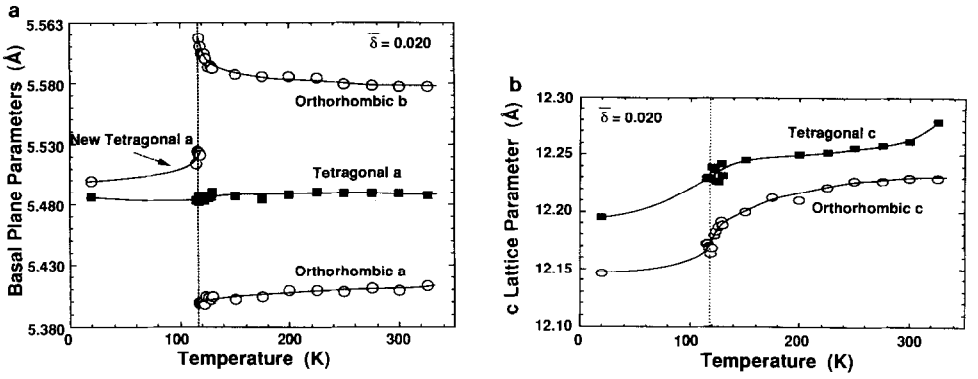

FIG. 8. Temperature dependences of the lattice parameters for the $\bar{\delta} = 0.020$ sample.

above 118 K. This strain behavior is noticeably different than that reported by Fernandez-Diaz *et al.*, who observe a more gradual onset of strain on heating, with the maximum strain occurring a few degrees after the structural transition. It is possible the discrepancies between the two reports may be due to differences arising from the use of single crystals in our case, and ceramic preparations in the other. Even though the *c* parameter decreases as *b* increases, the unit cell volume shows a large discontinuity at 118 K (Fig. 11), indicating the *Pccn* to $P4_2/ncm$ phase transition is first order. The tetragonal phase also appears to be influenced by the transition, as its unit cell volume increases sharply but continuously upon heating through 118 K, which may be caused by a subtle atomic rearrangement, or by strain resulting from structural registry with the transforming phase.

$Pr_2NiO_{4+\delta}$ samples annealed at $\log f_{O_2} = -8.18$ and -8.00 with $\bar{\delta} < 0.003$ were also examined by X-ray diffraction at room temperature and below, revealing complex phase behavior near the stoichiometric limit or reduction boundary. Both samples con-

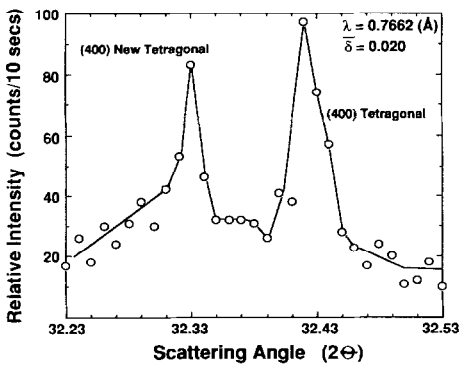

FIG. 9. (400) reflections showing two distinct tetragonal phases coexisting in $\bar{\delta} = 0.020$ at 19 K.

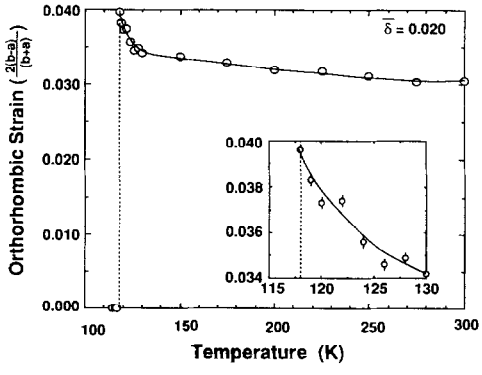

FIG. 10. Temperature dependence of the orthorhombic strain parameter ($s = 2(b - a)/(b + a)$) for $\bar{\delta} = 0.020$, with inset showing the strain near the structural transition.

tain a nonequilibrium assemblage of more than two K_2NiF_4 perovskite phases, suggesting that deviations from equilibrium occurred either during the anneal, or that the kinetics of the quench to room temperature are not fast enough to ensure a homogeneous sample. The diffusivity of oxygen in stoichiometric materials may be large enough that samples incorporate small amounts of excess oxygen on cooling before the quench kinetically limits oxygen transport. This would be surprising, however, since the annealing atmosphere contains little available oxygen in the cool region of the furnace. The presence of small amounts of the reduction products in one of the samples, the transparent amber color of the crystals, and the lack of evidence for any Ni^{3+} by iodometric titrations provide evidence that these samples are either highly stoichiometric or substoichiometric, $\delta < 0$. In addition to the complex assemblage of phases, the texturing effects observed in these data make it difficult to determine whether additional equilibrium phase separation regions actually exist at the low δ end of the phase diagram. Further characterization of these samples is currently in progress.

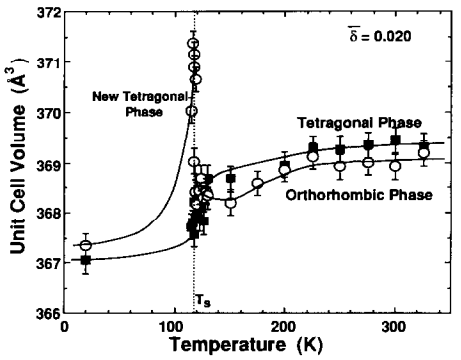

FIG. 11. Temperature dependences of the unit cell volume for both phases in the $\bar{\delta} = 0.020$ sample. The discontinuity in the orthorhombic phase volume is indicative of a first-order phase transition.

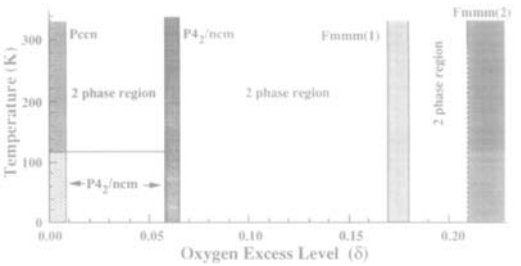

FIG. 12. Semiquantitative oxygen concentration phase diagram for $Pr_2NiO_{4+\delta}$. Shaded areas represent single-phase regions, and unshaded areas represent two-phase coexistence regions. The details of phase behavior near the stoichiometric limit remain poorly characterized and are not represented in this phase diagram.

Results of this investigation and our prior neutron diffraction study enable us to propose a semiquantitative oxygen stoichiometry phase diagram for $Pr_2NiO_{4+\delta}$, which is based on the observed lattice parameters, oxygen nonstoichiometry, relative phase volumes, and magnetic ordering temperatures of the samples (Fig. 12). The diagram is initially constructed around the $P4_2/ncm$–$Pccn$ miscibility gap, because the width of this region can be estimated from the relative amounts of the two phases in $\bar{\delta} = 0.020$ and $\bar{\delta} = 0.052$, along with the information that $Pr_2NiO_{4.060}$ is single-phase tetragonal. The $P4_2/ncm$–$Pccn$ phase separation region is estimated to encompass the excess oxygen range $0.005 < \delta < 0.058$. Having a nearly stoichiometric $Pccn$ phase is also consistent with the observation of this phase, among others, in the two samples showing no measurable excess oxygen which were annealed at $\log f_{O_2} = -8.18$ and -8.00. Below the structural transition at 118 K, two tetragonal $P4_2/ncm$ phases coexist. Although these phases have the same symmetry, their oxygen defect concentrations remain quite different, and are thus considered separate phases with distinct oxygen correlations. The compositional range of the single-phase $P4_2/ncm$ region is esti-

mated to be $0.058 < \delta < 0.065$, by assuming a linear dependence of the Néel temperature on oxygen content for tetragonal samples. Samples on the boundaries of the single-phase region have Néel temperatures of 143 and 56 K, and a single-phase sample, $Pr_2NiO_{4.060}$, shows T_N = 116 K (the Néel temperature of $Pr_2NiO_{4.064}$ has not yet been determined). The next phase separation region, between $P4_2/ncm$ and $Fmmm(1)$, is estimated to be $0.065 < \delta < 0.170$ on the basis of the relative amounts of the two phases in $\bar{\delta} = 0.162$, the maximum δ end of the single phase $P4_2/ncm$ region, and the single phase $Pr_2NiO_{4.17}$ sample. Because the lattice parameters of the $Fmmm(1)$ phase are almost identical in both two-phase regions in which it exists ($\bar{\delta} = 0.162$ and $\bar{\delta} = 0.195$), the width of its single-phase region is assumed to be quite small, on the order of 0.005–0.010. Preliminary studies of the temperature dependence of a phase-pure sample of the $Fmmm(1)$ phase show no low temperature phase transitions (*17*). The range of the phase separation region between the $Fmmm(1)$ and $Fmmm(2)$ phases is expected to be roughly $0.18 < \delta < 0.21$, with the single phase region of the second $Fmmm$ phase appearing in the range $0.21 < \delta < 0.22$. The high δ $Fmmm$ phase appears to be the most nonstoichiometric K_2NiF_4-structured phase, as it also coexists at the oxidation boundary with $Pr_4Ni_3O_{10}$ and $PrO_{1.83}$. The low temperature behavior of $Fmmm(2)$ has yet to be investigated, and is merely represented as a dashed line in Fig. 12. Further characterization of the oxygen concentration phase diagram at low and high temperatures, including a detailed investigation of the stoichiometric region and of phase transitions, is currently in progress. In order to more clearly illustrate the trends of the lattice parameters and unit cell of volume of $Pr_2NiO_{4+\delta}$ as a function of excess oxygen, Fig. 13 presents the room temperature values with respect to oxygen nonstoichiometry. Dotted lines through two phase regions are provided as guides to assist in identifying trends, and the dashed line in Fig. 13a serves to connect the average of the basal plane parameters (open circles). The single-phase lattice parameters are included, although the exact position of the $Pccn$ phase is unknown. The average of the basal plane lattice parameters decreases within and between phases with increasing δ, as expected from the accompanying increase in trivalent nickel content, while the c parameter increases with δ (Fig. 13b). Also, with the exception of the range between the $Pccn$ and the $P4_2/ncm$ phases, the unit cell volume of $Pr_2NiO_{4+\delta}$ decreases with increasing δ (Fig. 13c). These roughly linear changes in lattice parameters with increasing excess oxygen are consistent with Vergard's rule.

Discussion

The presence of multiple phase separation regions in the oxygen concentration phase diagram of $Pr_2NiO_{4+\delta}$ highlights the importance of oxygen defects in determining the structure and properties in this family of layered oxides. Although the defect or concomitant hole correlations associated with excess oxygen in $Pr_2NiO_{4+\delta}$ appear to drive the phase separations, the thermodynamic details of this behavior remain unclear. Large concentrations of interstitial oxygen ions appear to be stabilized by the accompanying decrease in charge separation between the electronegative MO_2 planes and the electropositive $(LnO)_2$ isolation bilayers. At moderate and low temperatures (below 700 K), relatively high densities of interstitial oxygen may lead to short range correlated distributions of defects or holes, or larger long range ordered supercells, rather than the random distributions present at higher temperatures. The correlation of these defects from steric and/or coulombic effects may drive a separation into oxygen-rich and -poor phases to yield a minimum in

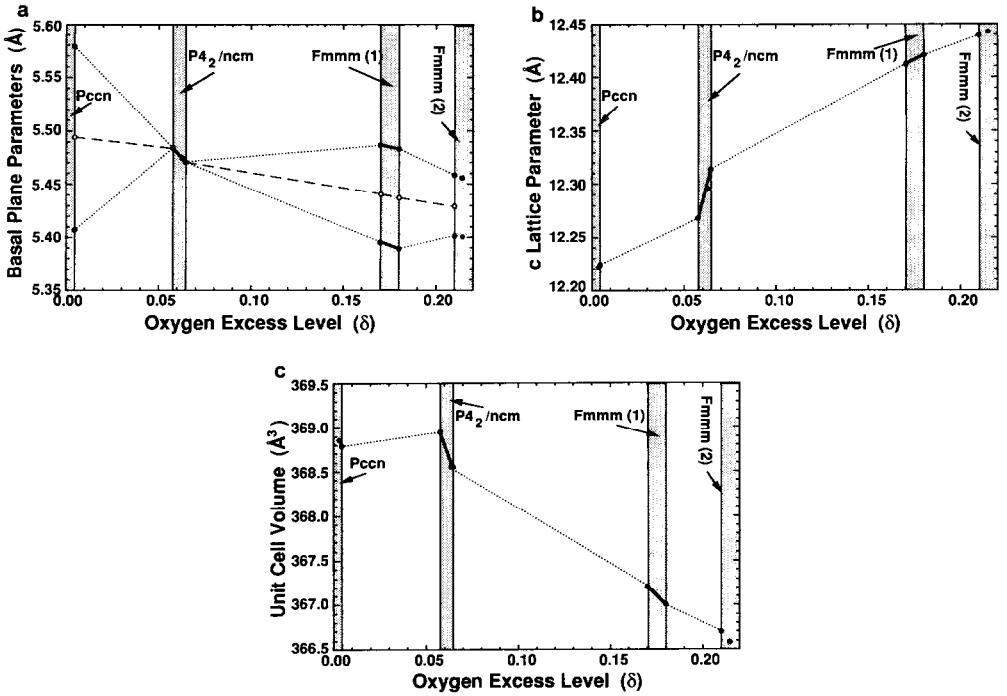

FIG. 13. Room temperature lattice parameters and unit cell volume dependence on excess oxygen in $Pr_2NiO_{4+\delta}$. Dotted lines connect parameters across two-phase regions, dashed lines and open circles represent the average basal plane lattice parameter for each phase.

the overall free energy by spinodal decomposition. It is expected that no phase separations and smaller maximum defect concentrations would be present in K_2NiF_4-type oxides where there is no appreciable charge separation, as in Ca_2MnO_4, or even in heavily substituted $Ln_{2-x}A_xMO_4$ (A = alkaline earth) materials where the charge separation is reduced.

$Pr_2NiO_{4+\delta}$ seems to be an ideal material for studying the influence of oxygen defects on phase separations, because its multiple and broad miscibility gaps appear to separate highly restricted and stable concentrations of interstitial oxygen. It may serve as a general oxygen concentration phase diagram for all K_2NiF_4-structured oxides, although certain phase separation regions appear to be suppressed or subtly altered in some oxides such as $La_2CuO_{4+\delta}$ and $La_2NiO_{4+\delta}$. By analogy with the highly nonstoichiometric phases of $La_2CuO_{4+\delta}$ and $La_2NiO_{4+\delta}$ (6, 2), the defects in the nonstoichiometric *Fmmm* phases of $Pr_2NiO_{4+\delta}$ are expected to be located at or near the (1/4, 1/4, 1/4) interstitial sites. The lack of unambiguous superlattice reflections (within the sensitivity limit of the present synchrotron X-ray diffraction study) from these "*Fmmm* phases" suggests the presence of only short range or incommensurate lattice distortions, or perhaps a larger supercell. On the other hand, the correlations of oxygen defects in the more stoichiometric phases of $Pr_2NiO_{4+\delta}$ are either commensurate or not strong enough to disrupt long range lattice distortions. The small concentrations of oxygen defects actually present make it difficult to resolve the defect location. It appears that there is a delicate balance among long range

lattice distortions, oxygen defect concentrations, and oxygen defect correlations that energetically determine the structure of the oxide. In addition to the presence of multiple phase separation regions, $Pr_2NiO_{4+\delta}$ may also serve as a model oxide because these separations are not kinetically limited as may be the case in $La_2NiO_{4+\delta}$. Jorgensen *et al.* (*2*) report that $La_2NiO_{4+\delta}$ separates into an *Fmmm* phase with $\delta \approx 0.12$ and a *Bmab* phase with $\delta \approx 0.02$ after a low temperature anneal (500°C). However, rapid quenching of a $La_2NiO_{4+\delta}$ sample from 1200°C results in a single *I4/mmm* phase (*7*) with $\delta = 0.07$, which falls inside the low temperature *Bmab–Fmmm* phase separation envelope (*2*). This implies that the kinetics of interstitial oxygen diffusion in $La_2NiO_{4+\delta}$ at the onset temperature of phase separation may be slow compared with the rapid quench rate, and that it is possible to prevent phase separation by apparently locking in a "glassy" distribution of thermally randomized defects. This phenomenon has not been observed for any $\bar{\delta}$ of $Pr_2NiO_{4+\delta}$, presumably due to much larger oxygen diffusivities at the temperature of the onset of phase separation than in $La_2NiO_{4+\delta}$.

Acknowledgments

We acknowledge many helpful discussions with our colleagues at the University of Delaware and Brookhaven National Laboratory. This investigation was supported by the National Science Foundation (DMR-8914080). Research at Brookhaven National Laboratory was also partially supported by the Division of Material Science, U.S. Department of Energy, under Contract DE-AC02-76CH00016.

References

1. J. D. Jorgensen, B. Dabrowski, S. Pei, D. G. Hinks, L. Soderholm, B. Morosin, J. E. Schirber, E. L. Venturini, and D. S. Ginley, *Phys. Rev. B* **38,** 11337 (1988).
2. J. D. Jorgensen, B. Dabrowski, S. Pei, D. R. Richards, and D. G. Hinks, *Phys. Rev. B* **40,** 2187 (1989).
3. B. Dabrowski, J. D. Jorgensen, D. G. Hinks, S. Pei, D. R. Richards, K. G. Vandervoort, G. W. Crabtree, H. B. Vanfleet, and D. L. Decker, unpublished.
4. D. J. Buttrey, J. D. Sullivan, G. Shirane, and K. Yamada, *Phys. Rev. B* **42,** 3944 (1990).
5. D. J. Buttrey, P. Ganguly, J. M. Honig, C. N. R. Rao, R. R. Schartman, and G. N. Subanna, *J. Solid State Chem.* **74,** 233 (1988).
6. C. Chaillout, S. W. Cheong, Z. Fisk, M. S. Lehmann, M. Marezio, B. Morosin, and J. E. Schirber, *Physica C* **158,** 183 (1989).
7. T. Freltoft, D. J. Buttrey, G. Aeppli, D. Vaknin, and G. Shirane, *Phys. Rev. B* **44,** in press (1991).
8. R. Saez-Puche, F. Fernandez, J. Rodriguez-Carvajal, and J. L. Martinez, *Solid State Commun.* **72,** 273 (1989).
9. D. J. Buttrey and J. M. Honig, *J. Solid State Chem.* **72,** 38 (1988).
10. P. Ganguly, S. Kollali, C. N. R. Rao, and S. Kern, *Magn. Lett.* **1,** 107 (1980).
11. D. J. Buttrey, H. R. Harrison, J. M. Honig, and R. R. Schartman, *J. Solid State Chem.* **54,** 407 (1984).
12. D. J. Buttrey and J. M. Honig, submitted for publication.
13. D. E. Rice, D. J. Buttrey, W. E. Farneth, and D. G. Swartzfager, in preparation.
14. Swanson *et al., Natl. Bur. Stand. Annu Rep.,* 2779 (1953).
15. C. Chaillout, J. Chenavas, S. W. Cheong, Z. Fisk, M. Marezio, B. Morosin, and J. E. Schirber, *Physica C,* in press (1991).
16. M. T. Fernandez-Diaz, J. Rodriguez-Carvajal, J. L. Martinez, G. Fillion, F. Fernandez, and R. Saez-Puche, *Z. Phys. B* **82,** 275 (1991).
17. J. D. Sullivan, D. J. Buttrey, D. E. Cox, and J. Hriljac, in preparation.